Review of Scientific Instruments ARTICLE scitation.org/journal/rsi

Simulations of wavelength-multiplexed holography for single-shot spatiotemporal characterization of NIF's advanced radiographic capability (ARC) laser

Cite as: Rev. Sci. Instrum. 92, 053003 (2021); doi: 10.1063/5.0043659
Submitted: 10 January 2021 • Accepted: 17 April 2021 •
Published Online: 7 May 2021

E. Grace,[1,2,a)] T. Ma,[2] Z. Guang,[1] D. Alessi,[2] S. Herriot,[2] M. Rhodes,[2] J. Park,[3] and R. Trebino[1]

AFFILIATIONS

[1] School of Physics, Georgia Institute of Technology, 837 State St. NW, Atlanta, Georgia 30332, USA
[2] Lawrence Livermore National Laboratory, 7000 East Ave., Livermore, California 94550, USA
[3] Electrical and Computer Engineering, Colorado State University, 400 Isotope Dr., Fort Collins, Colorado 80523, USA

Note: Paper published as part of the Special Topic on Proceedings of the 23rd Topical Conference on High-Temperature Plasma Diagnostics.
[a)] **Author to whom correspondence should be addressed:** esgrace@gatech.edu

ABSTRACT

We simulate the use of a newly developed single-shot wavelength-multiplexed holography-based diagnostic, STRIPED FISH, to fully characterize the as-delivered laser pulses of the National Ignition Facility's Advanced Radiographic Capability (NIF-ARC) laser. To that end, we have performed simulations of the NIF-ARC pulse incorporating (a) a time-integrated spatial-profile measurement and a complete temporal-intensity-and-phase measurement using a frequency resolved optical gating, but without any spatiotemporal pulse characterizations, and (b) simulated first-order spatiotemporal distortions, which could be measured on a single shot if a STRIPED FISH device were deployed.

I. INTRODUCTION

High-intensity laser–matter interactions at or near a focus depend delicately upon the laser pulse intensity and phase, and distortions in the pulse can produce undesirable and unexpected target physics.[1,2] In particular, spatiotemporal distortions, which involve the coupling of the laser intensity and phase as a function of space and time, can have deleterious effects on the focal spot peak intensity. The most common spatiotemporal distortions are first-order distortions, which include the pulse front tilt, spatial chirp, and angular dispersion, as well as the less-known phase couplings such as wavefront rotation and wave-front tilt dispersion. However, higher-order spatiotemporal distortions can also occur, resulting in a spatiotemporally complex pulse.[3] The regenerative amplification process in a chirped pulse amplifier (CPA) can exacerbate the existing spatiotemporal distortions and introduce intensity-dependent coupling effects.[4–8] Multi-stage amplification in petawatt-scale laser systems, such as the National Ignition Facility's Advanced Radiographic Capability laser (NIF-ARC)[9–11] where 13 Nd:phosphate glass amplifiers are used to achieve energies up to 1.0 kJ per 38 ps beamlet and 250 J in a 1.3 ps beamlet, is no exception. Achieving and maintaining the highest output intensity requires precise control of the temporal duration and focal spot of the pulse.

In order to optimize these pulses, a complete spatiotemporal pulse measurement technique is crucial. Even in the presence of the simplest first-order spatiotemporal couplings, the pulse cannot be completely revealed by a method that measures the spatial and temporal components separately.

For the NIF-ARC, which is capable of firing 1–2 shots per day and can change its laser parameters to accommodate various experimental requirements, the full characterization of its pulses is a complex task. To further complicate the measurement, high-intensity laser sources are particularly vulnerable to shot-to-shot instabilities, which can contaminate experimental data.

Conventional laser measurement techniques, including spatial profilers, time-averaged power meters, and spectrometers, are not capable of capturing the spatiotemporal complexity of the pulse. Furthermore, most pulse diagnostics that do measure the spatiotemporal field must scan a parameter such as the delay or transverse position and so must average over many pulses, missing any pulse-to-pulse variations.[12–22]

To address this problem, we have developed a complete, single shot, spatiotemporal pulse diagnostic, Spatially and Temporally Resolved Intensity and Phase Evaluation Device: Full Information from a Single Hologram (STRIPED FISH), which measures the spatiospectral pulse field $E(x, y, \omega)$ on a single shot and directly yields the full spatiotemporal field $E(x, y, z, t)$ from a Fourier transformation and diffraction integral. Previous work has demonstrated the ability of STRIPED FISH to accurately characterize the simultaneous pulse front tilt and spatial chirp,[23] the ultrafast lighthouse effect,[24] multimode optical fiber outputs,[25,26] complex waveforms in free space,[27,28] and a terawatt laser source.[29] The simulations contained here showcase the ability of STRIPED FISH to distinguish and predict the focal behavior of spatiotemporal distortions that may exist unmeasured on the NIF-ARC laser.

II. PRINCIPLES OF STRIPED FISH

STRIPED FISH measures $E(x, y, \omega)$ on a single shot by simultaneously generating multiple spatial holograms of the unknown pulse at different frequencies (see Fig. 1). It takes the measurement with respect to a reference pulse, which is generated by spatially filtering a portion of the unknown beam and temporally characterizing it using a GRENOUILLE (GRating-Eliminated No-nonsense Observation of Ultrafast Incident Laser Light E-fields).[30] The reference pulse and the unknown pulse cross at a small vertical angle on a two-dimensional diffractive optical element (DOE), which generates an array of crossed beam pairs. The DOE is chosen so that the angular dispersion within the orders used by STRIPED FISH is negligible and only serves to replicate the original beam pair, and it is rotated around the optic axis so that each beam pair's horizontal angle is unique. The array is then sent through a narrow-band interference band pass filter (IBPF), which is rotated horizontally at an angle with respect to the optic axis so that the transmitted center frequency depends primarily on the horizontal incidence angle (the vertical angle effect is minimal, decided by the angle-tuning feature in IBPF). After the IBPF, each beam pair in the array has a unique frequency. Finally, the resulting array of quasi-monochromatic holograms is imaged onto a camera sensor, where the beam pairs cross to produce spatial fringes. All the holograms are recorded simultaneously on a single camera frame.

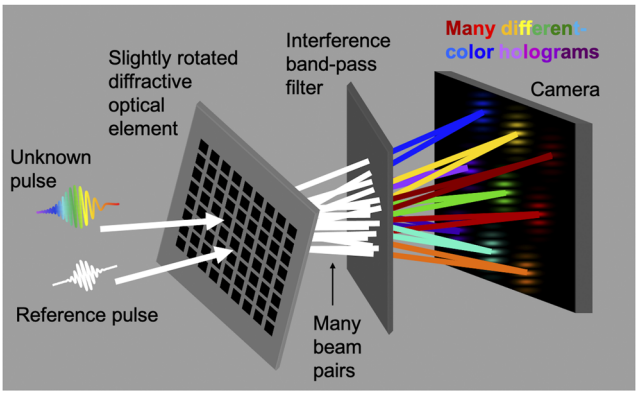

FIG. 1. Schematic of the STRIPED FISH device. The DOE is rotated at ~10° to give angular separation of beam pairs in the horizontal direction, and the IBPF is tilted at 25°–35° to allow certain transmission wavelengths. Adapted with permission from P. Zhu *et al.*, Opt. Express **25**, 24015–24032 (2017). Copyright 2017 Optical Society of America.

Since the reference pulse is spatiotemporally characterized, the unknown pulse's spatiospectral field can be extracted from the spatial fringes according to the following basic equation of holography:[31]

$$I(x,y,\omega) = |E_{unk}(x,y,\omega)|^2 + |E_{ref}(x,y,\omega)|^2 + E_{unk}(x,y,\omega)E^*_{ref}(x,y,\omega)e^{iky\,sin(\alpha)} + E^*_{unk}(x,y,\omega)E_{ref}(x,y,\omega)e^{-iky\,sin(\alpha)}, \quad (1)$$

where E_{unk} is the unknown pulse to be measured, E_{ref} is the known reference pulse, and α is the crossing angle between the two beams. The third term contains $E_{unk}(x, y, \omega)$, the field information as a function of transverse position and frequency in each hologram, and the complex conjugate of the characterized reference pulse field. The unknown field is extracted by collecting the transverse field profiles for each hologram and using the relative spectral phase information from the reference pulse field. Then, the unknown field $E_{unk}(x, y, \omega)$ is inverse Fourier transformed from frequency to time to produce $E_{unk}(x, y, t)$. The remaining pulse field dependence on z (see Figs. 4–6) is obtained by computing diffraction integrals using the Rayleigh–Sommerfeld solution.[32] The result is a complete spatiotemporal measurement of $E_{unk}(x, y, z, t)$ from a single camera frame.[23–29,33,34]

III. SPATIOTEMPORAL SIMULATIONS OF NIF-ARC LASER SYSTEM

Previous data taken on the NIF-ARC laser system (see Fig. 2) includes the time-integrated spatial profile and the single-shot temporal and spectral intensity and phase characterization by the Frequency Resolved Optical Gating (FROG). For the following simulations, we used spatial profile data for the beam B353a at ARC. These data are important but do not contain spatiotemporal coupling information. In order to display the information that could be illuminated with a spatiotemporal measurement, we add spatiotemporal distortions to these temporal and spatial measurements and propagate the resulting fields through a focus.

First, the time-integrated spatial intensity data $I(x, y)$ and spectral electric field data $E(\omega)$ as measured by using a single-shot GRENOUILLE device (see Fig. 2) are directly multiplied with a flat zero spatial phase assumed to produce a separable, spatiotemporal-coupling free electric field: $E(x, y, \omega) = E(x, y)E(\omega)$, where $E(x, y) \propto [I(x, y)]^{1/2}$ (see Fig. 3). To simulate ideal achromatic focusing, this field is assigned a curved wavefront and propagated through the focal spot (see Fig. 4). Although the beam undergoes diffraction as it propagates, the focal spot is spatiotemporally undistorted.

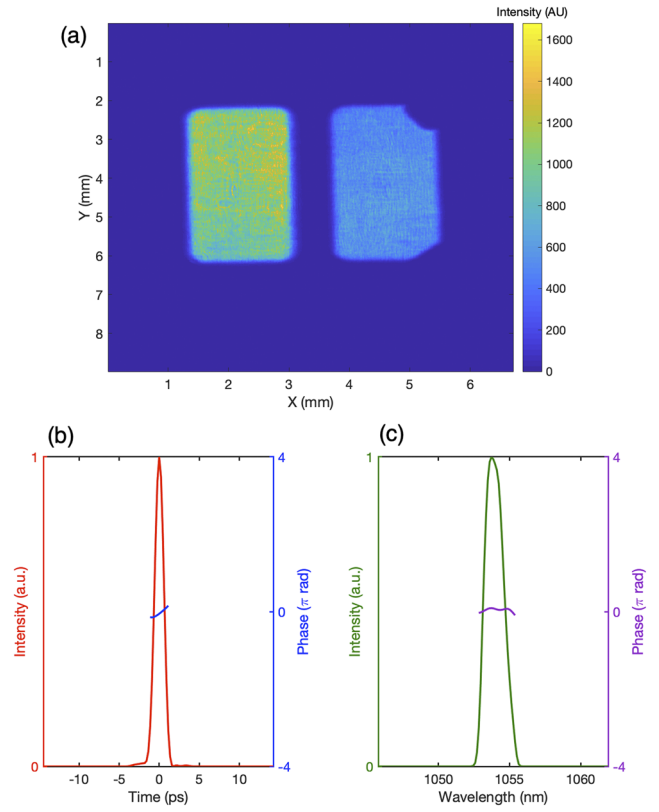

FIG. 2. Data taken from ARC shot N190523-001-999 for beam B353: (a) time-integrated spatial profile for beam B353b (left) and B353a (right), (b) FROG-measured temporal intensity and phase for B353a, and (c) FROG-measured spectrum and spectral phase for B353a.

In the spatiotemporal domain, the expression for the first-order coupled field is

$$E(x,t) \propto \exp\{Q_{xx}x^2 + 2Q_{xt}xt - Q_{tt}t^2\}, \tag{2}$$

where Q_{xt} is the coupling coefficient between space and time. The real parts of Q_{xx} and Q_{tt} describe the beam spot size and the pulse duration, while their imaginary components give the wavefront curvature and the temporal phase, respectively. The real part of the coupling coefficient Q_{xt} is the pulse front tilt, which can cause one side of the beam to arrive before the other side, and the imaginary part is wavefront rotation, which describes how the phase fronts change direction in time as the pulse propagates. As in Ref. 32, we normalize the spatiotemporal couplings to pulse parameters. We define the normalized form of the spatiotemporal amplitude coupling as

$$\mathrm{Re}\{Q_{xt}\} = \rho[-\mathrm{Re}\{Q_{xx}\}\mathrm{Re}\{Q_{tt}\}]^{1/2}, \tag{3}$$

where ρ is a normalized, dimensionless parameter that assigns the strength of the spatiotemporal coupling term with an absolute value between 0 and 1.[35] In the spatiotemporal domain,

$$\rho = \frac{\iint dxdtI(x,t)xt}{\Delta x \Delta t}. \tag{4}$$

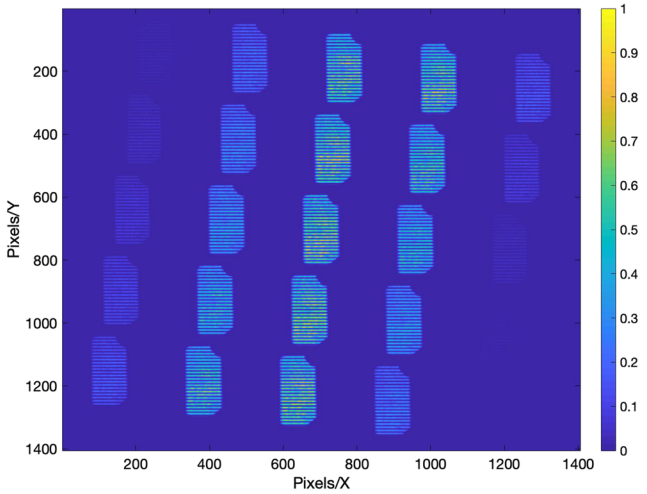

FIG. 3. Simulated STRIPED FISH trace for the ARC shot N190523-001-999 for beam B353a with no spatiotemporal distortions added. In this trace, we use 25 holograms, each with a different monochromatic frequency. As a set, the holograms' frequencies evenly sample over the measured NIF-ARC spectrum (see Fig. 2). Each beamlet is produced using Eq. (1) at one of the specified frequencies with a separable, spatiotemporal-coupling free electric field. Our previous work has simulated the effect of various spatiotemporal couplings on STRIPED FISH traces.[30]

For all simulations, the value of ρ was kept at 0.35, which corresponds to a relatively low coupling that we expect to see in experiment. Due to the relationship between the real and imaginary components of the various spatiotemporal couplings,[36] we define

$$\mathrm{Im}\{Q_{xt}\} = 2\rho[-\mathrm{Re}\{Q_{xx}\}\mathrm{Re}\{Q_{tt}\}]^{1/2}, \tag{5}$$

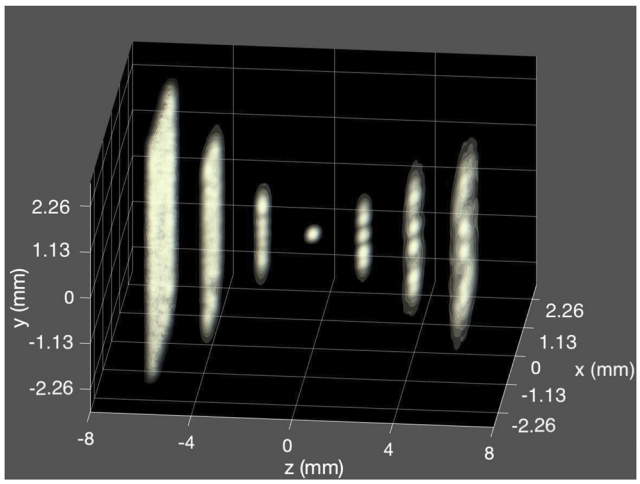

FIG. 4. Propagation of the spatiotemporally uncoupled ARC pulse through an ideal achromatic focus. Brightness indicates pulse intensity, and because the phase is responsible for the frequency distribution, the color distribution represents phase information. We set z = 0 mm at the focus, which is 8 mm from the STRIPED FISH measurement plane. Although the beam diffracts as it propagates, the focal spot is undistorted.

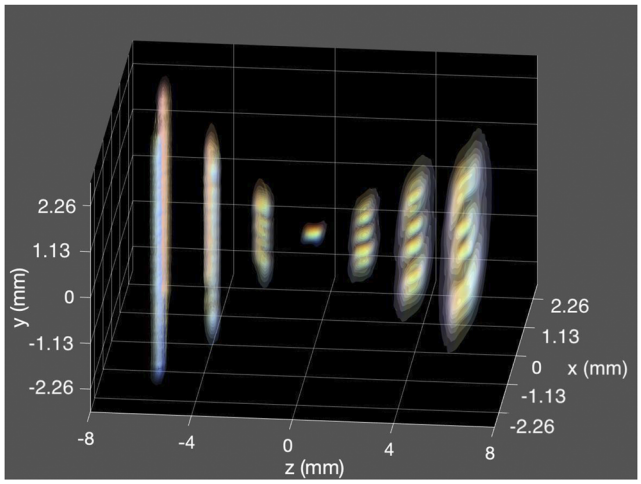

FIG. 5. Ideal achromatic focusing behavior of the ARC beamlet with a simulated first-order pulse front tilt with a relatively low strength of $\rho = 0.35$ that could be seen in the experiment. In the far-field, the pulse arrives as a function of angle, a phenomenon known as the lighthouse effect.

a choice that produces imaginary coupling strengths similar to those of real couplings.[32] Using these definitions, the ideal achromatic focusing of the ARC pulse with the simulated pulse front tilt is plotted (see Fig. 5). Pulse front tilt, or $\mathrm{Re}[Q_{xt}]$, is commonly caused by angularly dispersive elements such as prisms and diffraction gratings.[37] When a beam with pulse front tilt is focused, the focused pulse's wave vector $\vec{k}$ acquires a temporal dependence, a phenomenon usually referred to as the ultrafast lighthouse effect.[24,36,38] In other words, a distortion in the $x - t$ domain becomes a distortion in the $k_x - t$ domain at a focus: the wavevectors acquire a temporal dependence. At the target, a pulse with initial pule-front-tilt will spread in time, arriving as a function of angle.

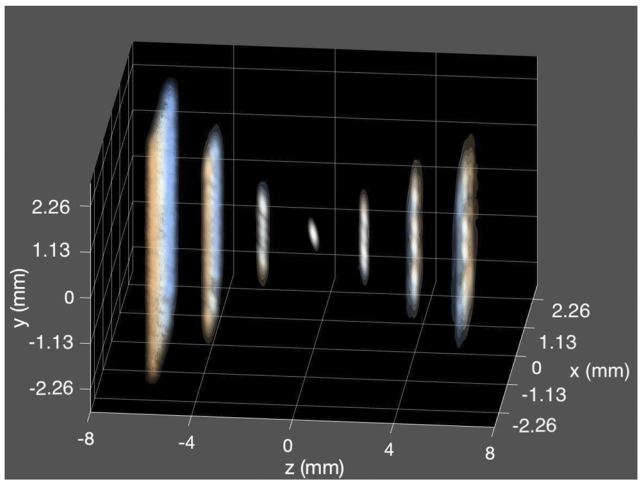

FIG. 6. Ideal achromatic focusing behavior of the ARC beamlet with simulated first-order wavefront rotation with a strength of $\rho = 0.35$. At a focus, the beam acquires an angular temporal chirp.

Practically, in addition, since the NIF-ARC laser system involves propagation through a number of full aperture lenses, it accumulates radial group delay, an effect similar to the pulse front tilt. In this case, the outer portion of the beam arrives before the inner portion of the beam. Analogous to the pulse front tilt, at the focus, this phenomenon results in the coupling of the radial propagation direction k_r and time. This effect can produce a longer pulse duration and diminished focal spot intensity.[39–43]

Finally, we simulate the ideal achromatic focusing behavior of a pulse with wavefront rotation (Fig. 6), or $\mathrm{Im}[Q_{xt}]$. Wavefront rotation is caused by a spatial chirp alone and/or the combination of a pulse front tilt and a temporal chirp,[36] all of which are common distortions that can be introduced by diffraction gratings. At a focus, the temporal dependence of the spatial phase (wavefront rotation) evolves into the temporal dependence of the propagation direction (angular temporal chirp).

IV. CONCLUSION

High-intensity laser–target interactions require precise tuning of the spatial and temporal characteristics of the laser pulse for optimal performance. Common spatiotemporal distortions can produce surprising and undesirable behavior at a focus, which can lead to contaminated data. At the high-intensity laser system NIF-ARC, which is of necessarily low-repetition-rate, a single-shot spatiotemporal diagnostic is required to fully assess the as-delivered focal spot. A single-shot STRIPED FISH diagnostic installed on the ARC beamline would act as a source of active feedback to identify the source of spatiotemporal distortions, including the pulse front tilt and wavefront rotation, and correct them before they reach the target.

ACKNOWLEDGMENTS

This work was performed under the auspices of the U.S. Department of Energy by Lawrence Livermore National Laboratory under Contract No. DE-AC52-07NA27344, supported, in part, by the LDRD (Grant No. 17-ERD-039), the DOE Early Career (Grant No. SCW1651), and the National Science Foundation under Grant No. ECCS-1609808. R.T. discloses that he owns a company that sells pulse-measurement devices.

DATA AVAILABILITY

The data that support the findings of this study are available from the corresponding author upon reasonable request.

REFERENCES

[1] D. H. Froula *et al.*, Nat. Photonics **12**, 262 (2018).
[2] M. Malinauskas *et al.*, Light: Sci. Appl. **5**, e16133 (2016).
[3] S. Akturk *et al.*, J. Opt. **12**, 093001 (2010).
[4] A. Giree *et al.*, Opt. Express **25**, 3104 (2017).
[5] G. Pretzler *et al.*, Appl. Phys. B **70**, 1 (2000).
[6] J. Bromage *et al.*, Opt. Lett. **35**, 2251 (2010).
[7] A. Zaukevičius *et al.*, J. Opt. Soc. Am. B **28**, 2902 (2011).
[8] O. Isaienko and E. Borguet, J. Opt. Soc. Am. B **26**, 965 (2009).
[9] C. A. Haynam *et al.*, Appl. Opt. **46**, 3276 (2007).
[10] J. K. Crane *et al.*, J. Phys.: Conf. Ser. **244**, 032003 (2010).

[11] J. M. DiNicola *et al.*, Proc. SPIE **9345**, 934501 (2015).
[12] P. Bowlan *et al.*, Opt. Express **15**, 10219 (2007).
[13] P. Bowlan *et al.*, Opt. Express **16**, 13663 (2008).
[14] P. Bowlan *et al.*, J. Opt. Soc. Am. B **25**, A81 (2008).
[15] P. Saari *et al.*, Lith. J. Phys. **20**, 948 (2010).
[16] P. Saari *et al.*, Lith. J. Phys. **50**, 121 (2010).
[17] P. Bowlan and R. Trebino, J. Opt. Soc. Am. B **29**, 244 (2012).
[18] J. Cohen *et al.*, IEEE J. Sel. Top. Quantum Electron. **18**, 218 (2012).
[19] A. Borot and F. Quéré, Opt. Express **26**, 26444 (2018).
[20] A. Jeandet *et al.*, J. Phys.: Photonics **1**, 035001 (2019).
[21] M. Rhodes *et al.*, Appl. Sci. **7**, 40 (2017).
[22] R. Trebino *et al.*, J. Appl. Phys. **128**, 171103 (2020).
[23] P. Gabolde and R. Trebino, Opt. Express **14**, 11460 (2006).
[24] Z. Guang *et al.*, J. Opt. Soc. Am. B **33**, 1955 (2016).
[25] Z. Guang *et al.*, Appl. Opt. **56**, 2060 (2017).
[26] P. Zhu *et al.*, Opt. Express **25**, 24015–24032 (2017).
[27] Z. Guang *et al.*, in *Frontiers in Optics/Laser Science* (Optical Society of America, Washington, DC, 2020), p. FTu6C.4.
[28] Z. Guang *et al.*, J. Opt. Soc. Am. B **31**, 2736 (2014).
[29] E. Grace *et al.*, in *Conference on Lasers and Electro-Optics* (Optical Society of America, Washington, DC, 2020), p. SM4H.6.
[30] P. O'Shea *et al.*, Opt. Lett. **26**, 932 (2001).
[31] J. Goodman, *Introduction to Fourier Optics*, 3rd ed. (Roberts & Company Publishers, Englewood, CO, 2005).
[32] M. Rhodes *et al.*, Appl. Opt. **56**, 3024 (2017).
[33] Z. Guang *et al.*, Appl. Opt. **54**, 6640 (2015).
[34] P. Gabolde and R. Trebino, J. Opt. Soc. Am. B **25**, A25 (2008).
[35] P. Gabolde *et al.*, Opt. Express **15**, 242 (2007).
[36] S. Akturk *et al.*, Opt. Express **13**, 8642 (2005).
[37] J. Hebling, Opt. Quantum Electron. **28**, 1759 (1996).
[38] F. Quéré *et al.*, J. Phys. B: At., Mol. Opt. Phys. **47**, 124004 (2014).
[39] Z. Bor, J. Mod. Opt. **35**, 1907 (1988).
[40] H.-M. Heuck *et al.*, Appl. Phys. B **84**, 421 (2006).
[41] J. Néauport *et al.*, Appl. Opt. **46**, 1568 (2007).
[42] E. W. Gaul *et al.*, Appl. Opt. **49**, 1676 (2010).
[43] S.-W. Bahk *et al.*, Opt. Lett. **39**, 1081 (2014).